

# Spectral bandwidth scaling laws and reconstruction of THz wave packets generated from two-color laser plasma filaments

A. D. Koulouklidis,<sup>1,2</sup> V. Yu. Fedorov,<sup>1,3,4</sup> and S. Tzortzakis<sup>1,2,4,\*</sup>

<sup>1</sup>*Institute of Electronic Structure and Laser (IESL), Foundation for Research and Technology - Hellas (FORTH), P.O. Box 1527, GR-71110 Heraklion, Greece*

<sup>2</sup>*Materials Science and Technology Department, University of Crete, 71003 Heraklion, Greece*

<sup>3</sup>*P. N. Lebedev Physical Institute of the Russian Academy of Sciences, 53 Leninskiy Prospekt, 119991 Moscow, Russia*

<sup>4</sup>*Science Program, Texas A&M University at Qatar, P.O. Box 23874 Doha, Qatar*

(Received 3 November 2015; published 24 March 2016)

We find the spectral bandwidth scaling laws of the THz wave packets, produced from two-color laser filaments, as a function of the input laser-pulse duration and demonstrate how one can fully recover the original broadband THz wave packets even using narrow-band detection techniques such as the widespread electro-optic sampling.

DOI: [10.1103/PhysRevA.93.033844](https://doi.org/10.1103/PhysRevA.93.033844)

## I. INTRODUCTION

Nowadays, electromagnetic fields in the THz frequency range are of interest for a wide range of applications, such as in spectroscopy, nondestructive testing, tomographic imaging, cultural heritage, and many others [1–6]. Modern THz sources are able to generate THz radiation with intensities high enough to observe nonlinear effects [7–9]. To date, there are two major techniques for the generation of intense THz pulses on tabletop setups: optical rectification in nonlinear crystals [10] and two-color filamentation (photoionization of gases by symmetry-broken laser fields) [11,12]. Optical rectification allows one to generate THz pulses with very high energies (up to 900  $\mu\text{J}$ ) and spectral widths up to 5 THz [13]. In turn, THz pulses generated by two-color filamentation have less energy (few  $\mu\text{J}$ ) but their spectrum is much broader, ranging from almost zero up to approximately 60 THz [14].

Although the generation of intense broadband THz radiation is a challenging task, its detection can be even more complicated. In the majority of THz applications, we need a way to coherently detect a pulsed THz wave with a simultaneous measurement of its amplitude and phase. The most commonly used coherent detectors for THz radiation are photoconductive antennas [15,16] and electro-optic (EO) crystals [17–19]. However, they have a limited detection bandwidth due to a finite carrier lifetime in antenna photoconductors and phonon resonances in EO crystals. A typical THz pulse emitted during two-color filamentation has a spectrum which extends far beyond the detection limits of these two types of detectors. To date, the most broadband method for coherent detection of THz radiation is air-biased coherent detection (ABCD) [20–22]. However, the ABCD method is less sensitive than EO detectors especially at low repetition rates, while its physical limitations have not been fully studied. As a consequence, the majority of laboratories still use the EO crystals as the main tool for coherent detection of THz radiation. However, since EO detectors can measure only a small part of the generated THz spectrum, the detected THz electric field is strongly distorted. As a result, during EO detection, much information about the spectral content, shape, and duration of the original THz wave

packet is lost, which is something that can negatively impact many applications.

Here we theoretically derive the scaling laws of the THz spectral bandwidth produced from two-color laser filaments as a function of the input laser-pulse duration and find the spectrum lossless limits for EO detection. Using this information, we perform experiments by stretching the input laser pulse to the lossless regime and then extrapolate the THz bandwidth and pulse duration at shorter input laser durations. Additionally, in order to also correct for the detector response function, we apply an iterative reconstruction algorithm that implements a numerical simulation of the EO detection. Using this approach, we are able to fully restore the original THz wave packet using only EO detection.

## II. THE EFFECT OF A LIMITED BANDWIDTH

First, let us demonstrate how the limited bandwidth of a detector affects our perception of a THz pulse. In our experiments, we generate THz pulses using the two-color filamentation scheme. Our Ti:sapphire chirped-pulse amplification laser system generates 40 fs pulses, at 800 nm central wavelength and maximum energy of 2.3 mJ. We focus the input laser pulse by a lens with 200 mm focal length, followed by a 50- $\mu\text{m}$ -thick  $\beta$ -barium borate (BBO) type-I crystal cut at a 29.9° angle, which generates the second harmonic. After the BBO crystal, at the focus of the lens, the two-color pulses create a plasma filament that emits THz radiation. In order to avoid the absorption in water vapor, we place our setup into a purge gas chamber filled with dry air. Using a pair of parabolic mirrors, we gather the emitted THz radiation in the far field and send it to a THz detector. To detect the generated THz pulses, we apply either EO detection or ABCD measurements. For EO detection, we use 0.5 mm zinc telluride (ZnTe) and 100  $\mu\text{m}$  gallium phosphide (GaP) crystals.

In addition to EO and ABCD measurements, we also conducted measurements of the generated THz pulses using Michelson interferometry (field autocorrelation) as a reference method. We should stress that although Michelson interferometry is not a method of coherent detection (it cannot explicitly measure the phase of a THz pulse), it allows one to detect the whole THz spectrum without limitations.

\*stzortz@iesl.forth.gr

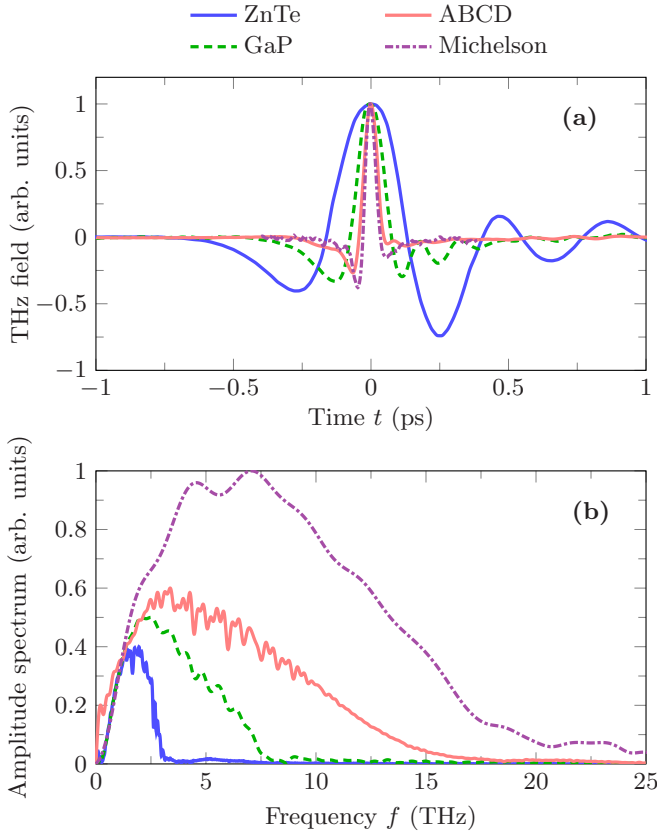


FIG. 1. (a) Normalized THz fields and (b) their amplitude spectra for a THz pulse measured by different techniques, namely, by ZnTe and GaP EO crystals as well as by the ABCD method and Michelson interferometry (the spectra are independently normalized appropriately for clarity reasons).

Figure 1 shows the THz fields and their amplitude spectra obtained by the different detection techniques. We see that the shortest spectrum is detected by the ZnTe crystal. It is followed by spectra measured by the GaP crystal and then by the ABCD measurement. The widest spectrum is registered by Michelson interferometry. The detection bandwidth of EO crystals is mainly restricted by their transverse optical phonon resonances. In ZnTe crystals, the first phonon resonance is located at 5.3 THz and in GaP at 11 THz [23]. In turn, the detection bandwidth of the ABCD method can be estimated as the inverse duration of the probe pulse (the main limiting parameter). In our experiments, the duration of the probe pulse is about 70 fs (the probe pulse is longer than the input pulse due to the dispersion in the guiding optics), which corresponds to a detection bandwidth of about 14 THz.

In Fig. 1, we also see that the THz field measured by the different detection techniques have different durations and shapes. Defining the THz pulse duration  $\tau_s$  as the full width at half maximum (FWHM) of the envelope of the modulus square of the detected THz field (measured signal), for the signals in Fig. 1 we have 420 fs for the ZnTe crystal, 157 fs for the GaP crystal, and 77 fs for the ABCD method. Finally, from the Michelson interferometry signal and spectrum and assuming a transform limited pulse we obtain  $\tau_s = 57$  fs, which can be safely considered as the shortest possible THz pulse duration in our experiments.

Thus, even using the best of our EO crystals, the measured THz pulse duration is two to three times larger than its real value. In addition, the signal from the EO detectors leads us to wrong conclusions about the shape of the original THz pulses. Figure 1 shows that both ZnTe and GaP crystals predict additional field oscillations that are absent on the signal measured by the more precise ABCD method. Thus, the EO detection, although it presents very high sensitivity, strongly affects our perception of the THz electric field, deforming its original shape and misleading us about its duration.

### III. SCALING LAWS FOR THE THz SPECTRAL BANDWIDTH

In this section, we find the laws according to which the spectral bandwidth and duration of the generated THz pulse depend on the duration of the input laser pulse. In order to find these laws, we use the well-accepted photocurrent model [24]. Since experimentally it is convenient to increase the laser-pulse duration by changing the distance between the gratings of the laser compressor, the resulting pulse becomes chirped. Therefore, to write the field of the main harmonic, we use the following expression:

$$E_{\omega_0}(t) = A_{\omega_0} \frac{\sqrt{1+iC}}{\sqrt{1+C^2}} \exp \left[ -(1+iC)2 \ln 2 \frac{t^2}{\tau_i^2} \right] e^{-i\omega_0 t},$$

where  $C$  is the chirp parameter, with  $\tau_i = t_i \sqrt{1+C^2}$  and  $t_i$  being the FWHM durations of the stretched and transform-limited input laser pulse. The field of the second harmonic is calculated as

$$E_{2\omega_0}(t) = \frac{\sqrt{I_{2\omega_0}/I_{\omega_0}}}{|E_{\omega_0}(t=0)|} E_{\omega_0}^2(t) e^{-i\pi/2},$$

where the prefactor is chosen in order to fix the ratio of the intensities  $I_{\omega_0} = n_0 \epsilon_0 c_0 A_{\omega_0}^2 / 2$  and  $I_{2\omega_0}$  of the main and second harmonic, respectively. The initial conditions in our calculations are  $E(t) = E_{\omega_0}(t) + E_{2\omega_0}(t)$ ,  $\lambda_0 = 800$  nm, and the intensity of the main and second harmonics is  $I_{\omega_0} = 5 \times 10^{13}$  W/cm<sup>2</sup> and  $I_{2\omega_0} = 0.2 I_{\omega_0}$ , respectively.

The photocurrent derivative  $\partial J / \partial t$  is calculated assuming that the medium consists of  $N_2$  molecules with the concentration  $2.68 \times 10^{19}$  cm<sup>-3</sup>. For the generated THz pulse, we consider a waveform that corresponds to the spectrum of  $\partial J / \partial t$  at frequencies below 100 THz.

Since the initial two-color pulse is chirped, we need to take into account that its phase is strongly modulated. Therefore, in order to avoid errors in calculations of the amount of free electrons, we use a phase-sensitive nonadiabatic ionization rate proposed by Yudin and Ivanov [25].

Figure 2 shows the dependence of the FWHM bandwidth of the power spectrum [Fig. 2(a)] and duration (inverse bandwidth) [Fig. 2(b)] of the generated THz pulse as a function of the FWHM duration  $\tau_i$  of the input laser pulse. The three curves correspond to three different initial (nonchirped) laser-pulse durations,  $t_i = 30, 40,$  and  $50$  fs, respectively, in order to show that the analysis is independent of the initial laser-pulse duration. One can see that the duration of the THz pulse has an astonishing simple linear dependence on the duration of the input laser pulse. Similar indications have

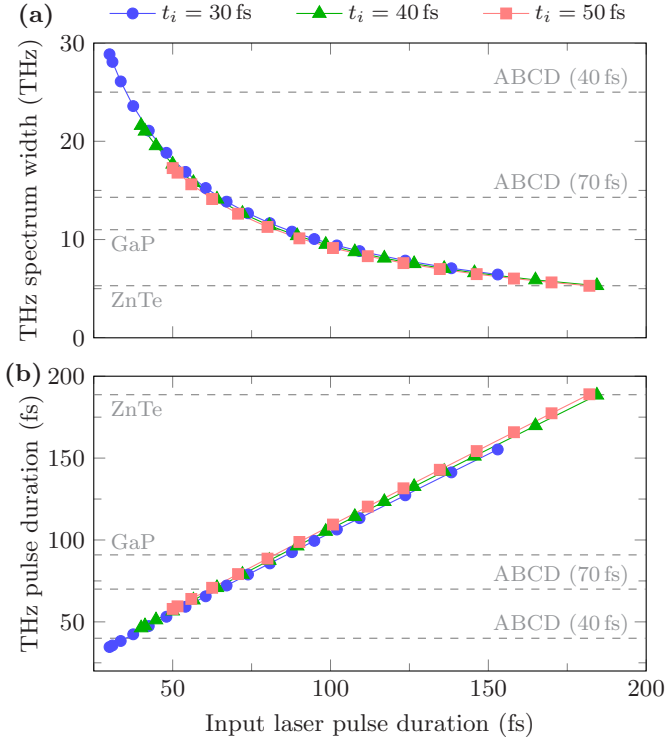


FIG. 2. The (a) dependence of the spectral bandwidth and (b) duration (inverse bandwidth) of the generated THz pulse on the FWHM duration  $\tau_i$  of the input laser pulse. Dashed lines indicate the limits of the various detection techniques. The ABCD method's limits are shown for two probe beam pulse durations, i.e., 70 and 40 fs.

been reported in [26]. In Fig. 2, we also have indicated the spectral bandwidth limits of the various techniques so one can easily identify what needs to be the laser-pulse duration in order to be within the limits of each detector. For instance, for EO detection with a GaP crystal, one should have laser-pulse durations above  $\sim 90$  fs and, for the ZnTe, above  $\sim 180$  fs.

Thus, from the previous discussion, it becomes clear which way we should proceed in order to find the duration of the THz pulse in our experiment. We need to stretch our input laser pulse above the duration that corresponds to the spectrum lossless detection regime, measure the THz pulse duration there, and then use the scaling laws we have just derived to find the corresponding THz pulse duration for shorter input laser pulses.

We need to stress though that even if the bandwidth of the EO detector is broad enough and one operates in the spectrum lossless regime, the THz pulse will still be distorted because of the chromatic dispersion and spectral sensitivity of the EO crystal. These effects, though, can be easily modeled and accounted for, as we show in the next section.

#### IV. THE RECONSTRUCTION METHOD

In this section, we introduce a reconstruction method whose aim is to restore the broadband THz wave packets that were distorted by the propagation through an EO detector (in the spectrum lossless case).

The EO sampling technique is based on measuring the birefringence induced by the THz field inside the detection crystal as a function of time. The technique has been extensively studied in the past, e.g., [23,27], and below we describe the methodology one needs to use to correctly model it.

A laser probe beam experiences polarization changes during its propagation through the detection crystal. After the crystal, the probe beam is split into two components with mutually perpendicular polarizations and sent to a pair of balanced photodiodes. Let us denote the voltage in each of the photodiodes as  $A_1$  and  $A_2$ . A normalized difference of  $A_1$  and  $A_2$  is given by [27]

$$\frac{A_1 - A_2}{A_1 + A_2} = \sin \Gamma, \quad (1)$$

where  $\Gamma$  is a relative phase shift between the two orthogonally polarized components of the probe beam. We can write  $\Gamma$  as [23]

$$\Gamma(t) = \frac{2\pi n_0^3 d}{\lambda_0} \text{Re}[F(t)], \quad (2)$$

where  $\lambda_0$  is the wavelength of the probe beam,  $n_0$  is the refractive index of the detection crystal at  $\lambda_0$ , and  $d$  is the crystal thickness. For a GaP crystal at  $\lambda_0 = 800$  nm, we have  $n_0 = 3.18$  [23]. The factor  $\text{Re}[F(t)]$  in Eq. (2) denotes the real part of the function  $F(t)$ , which we define as

$$F(t) = \frac{1}{2\pi} \int_{-\infty}^{\infty} H(\omega) \tilde{E}(\omega) e^{-i\omega t} d\omega. \quad (3)$$

Here,  $\tilde{E}(\omega)$  is the spectrum of the incoming THz pulse with electric field  $E(t)$ , that is,

$$\tilde{E}(\omega) = \int_{-\infty}^{\infty} E(t) e^{i\omega t} dt, \quad (4)$$

and  $H(\omega)$  is the EO response function, given by [23]

$$H(\omega) = r_{41}(\omega) G(\omega) T(\omega), \quad (5)$$

where  $r_{41}(\omega)$ ,  $G(\omega)$ , and  $T(\omega)$  are the frequency-dependent EO coefficient, the geometric response function, and the transmission coefficient of the detection crystal, respectively.

The transmission coefficient  $T(\omega)$  reads

$$T = \frac{t_1 t_2 e^{ikd}}{1 + r_1 r_2 e^{2ikd}}. \quad (6)$$

If we assume that the detection crystal is surrounded by dry air with a unity refractive index, then  $t_1 = 2/(1+n)$ ,  $t_2 = 2n/(n+1)$ , and  $r_1 = (1-n)/(1+n)$ ,  $r_2 = (n-1)/(n+1)$ , where  $n$  is the refractive index of the detection crystal at THz frequencies, with  $k = n\omega/c_0$  being the wave number of the THz pulse.

For the frequency-dependent refractive index  $n$ , we use the following model [23]:

$$n^2(\omega) = \varepsilon_{el} + \frac{S_0 \omega_0^2}{\omega_0^2 - \omega^2 - i\Lambda_0 \omega}. \quad (7)$$

In the case of GaP crystals,  $\varepsilon_{el} = 8.7$ ,  $S_0 = 1.8$ ,  $\omega_0/(2\pi) = 10.98$  THz, and  $\Lambda_0/(2\pi) = 0.02$  THz [23].

The geometric response function  $G(\omega)$  takes into account the mismatch between the phase velocity of the THz pulse and

group velocity  $v_g$  of the probe laser pulse inside the detection crystal [23]:

$$G(\omega) = \frac{1}{d} \int_0^d dz \int_{-\infty}^{\infty} \delta(z/v_g - t) e^{i(kz - \omega t)} dt \\ = \frac{1}{d} \frac{e^{i(k - \omega/v_g)d} - 1}{i(k - \omega/v_g)}. \quad (8)$$

For a probe pulse at  $\lambda_0 = 800$  nm propagating inside a GaP crystal,  $v_g = 0.28c_0$  [23].

The EO coefficient  $r_{41}$  determines the sensitivity of the detection crystal at different frequencies. We use the following model for  $r_{41}$  [23]:

$$r_{41}(\omega) = d_E \left( 1 + \frac{C \omega_0^2}{\omega_0^2 - \omega^2 - i \Lambda_0 \omega} \right), \quad (9)$$

with the same parameters  $\omega_0$  and  $\Lambda_0$  as in the model for  $n(\omega)$ . For GaP crystals,  $d_E = 1.13 \times 10^{-12}$  m/V and  $C = -0.47$ . These values of  $d_E$  and  $C$  differ slightly from the ones proposed in [23]. We modified the original values in order to shift the frequency where the real part of  $r_{41}$  becomes zero. This correction gives a better fit for our experimental data.

Equations (1)–(9) allow us to simulate the process of EO sampling for any given THz pulse. For an electric field  $E(t)$  of the initial THz pulse, the algorithm performs the following steps: (i) calculates the spectrum  $\tilde{E}(\omega)$  of  $E(t)$  in accordance with Eq. (4); (ii) using Eqs. (6)–(9), calculates the EO coefficient  $r_{41}(\omega)$ , the geometric response function  $G(\omega)$ , and the transmission coefficient  $T(\omega)$ ; (iii) calculates the EO response function  $H(\omega)$  from Eq. (5) and then the function  $F(t)$  from Eq. (3); (iv) using Eq. (2), calculates the phase shift  $\Gamma(t)$ . Finally, the sine of  $\Gamma$ , according to Eq. (1), gives us the EO signal that can be directly compared with the experimental data.

In order to choose a model for our THz pulse that enters the EO detection system, we turn to the results of the ABCD method (see Fig. 1). The signals show that the original THz pulse would be a single-cycle pulse, whose electric field  $E(t)$  can be modeled by the following function:

$$E(t) = E_0 \frac{t}{t_0} \exp\left(-\frac{t^2}{t_0^2}\right), \quad (10)$$

where  $E_0$  is the peak amplitude. The FWHM of the envelope of the modulus square of  $E(t)$  in (10) is  $\tau_0 = 1.81t_0$ .

To fit the experimental results, we use a nonlinear curve fitting process which runs iteratively, until convergence, the above algorithm with Eq. (10) as the initial condition and the only fitting parameters the duration  $\tau_0$  of the initial THz pulse and the thickness  $d$  of the EO crystal. We consider  $d$  as a fitting parameter in order to compensate for errors arising from inaccurate determination of the crystal's thickness together with possible misalignment of the crystal relative to the optical axis. As initial estimates for  $\tau_0$  and  $d$ , we use the duration of the recorded THz signal and the thickness of the EO crystal provided by its manufacturer. At this stage of the reconstruction, we do not take into account the absolute value of the amplitude  $E_0$  and we consider only normalized values.

In order to test our reconstruction method, we apply it to the signal measured by a  $100 \mu\text{m}$  GaP crystal and for an input laser pulse of 108 fs, which is in the spectrum lossless regime, as shown in Fig. 2.

In Fig. 3, we plot the experimentally measured THz signal (middle column) and its amplitude spectrum (right column) together with their best fits obtained by our reconstruction method for three different models of the initial pulse (left column). One can clearly see that the model from Eq. (10) (top row) gives the closest agreement with the experimental findings. The duration  $\tau_0$  of the original THz pulse, restored by our reconstruction method, is equal to 147 fs, while the duration of the experimental signal is 185 fs. Thus, if we provide spectrum lossless measurements, our reconstruction algorithm is able to nicely recover the shape and duration of the original THz pulse that was distorted by the propagation inside an EO crystal.

## V. RETRIEVAL OF THE ORIGINAL THz PULSE DURATION

In this section, we combine the analysis of Secs. III and IV in order to retrieve the duration of the THz pulse generated in our system by transform-limited laser pulses with duration of 40 fs. For this purpose, we conducted a series of experiments where we stretched our input laser pulses above durations that allow one to reach the detector spectrum lossless regime. For each experiment in the series, we measured the duration  $\tau_i$  of the input laser pulse and detected the corresponding generated THz pulses with a  $100 \mu\text{m}$  GaP crystal. Then, for the recorded EO signals that belong to the lossless regime of detection, we applied our reconstruction method and retrieved the duration  $\tau_0$  of the original THz pulse.

Figure 4 shows the duration  $\tau_s$  of the THz signal measured by the GaP crystal (blue dots) and the corresponding value  $\tau_0$  retrieved by our reconstruction method for laser-pulse durations  $\tau_i$  above 100 fs (green triangles). As a reference data, in this figure we also plot the duration  $\tau_s$  measured by the ABCD method (golden square) and the Michelson interferometer (purple pentagon) for the shortest initial laser pulse.

In Fig. 4, we see that for the input laser pulses whose duration  $\tau_i$  exceeds 100 fs, the values of  $\tau_0$  retrieved by our reconstruction method depend linearly on  $\tau_i$ , as expected from our theoretical results in Sec. III. Thus, we can confidently linearly extrapolate the THz pulse durations for the shorter laser-pulse durations, represented by the red triangles in Fig. 4. The obtained dependence of the THz pulse duration on the input laser-pulse duration is then given by

$$\tau_0 = a\tau_i + b, \quad (11)$$

with  $a = 1.16$  and  $b = 21.49$  (for  $\tau_0$  and  $\tau_i$  in femtoseconds). Using Eq. (11), we find that for our shortest initial laser pulse ( $\tau_i = 40$  fs), the generated THz pulse has duration of  $\tau_0 = 68$  fs. This value is between the duration of 57 fs estimated by the Michelson interferometry and the ABCD measurement of 77 fs, as could be expected.

One may consider that Eq. (11) is specific to our experimental conditions only. In order to verify this point, we performed additional simulations, as the ones described in Sec. III, for different laser peak intensities, in the range  $I_{\omega_0} =$

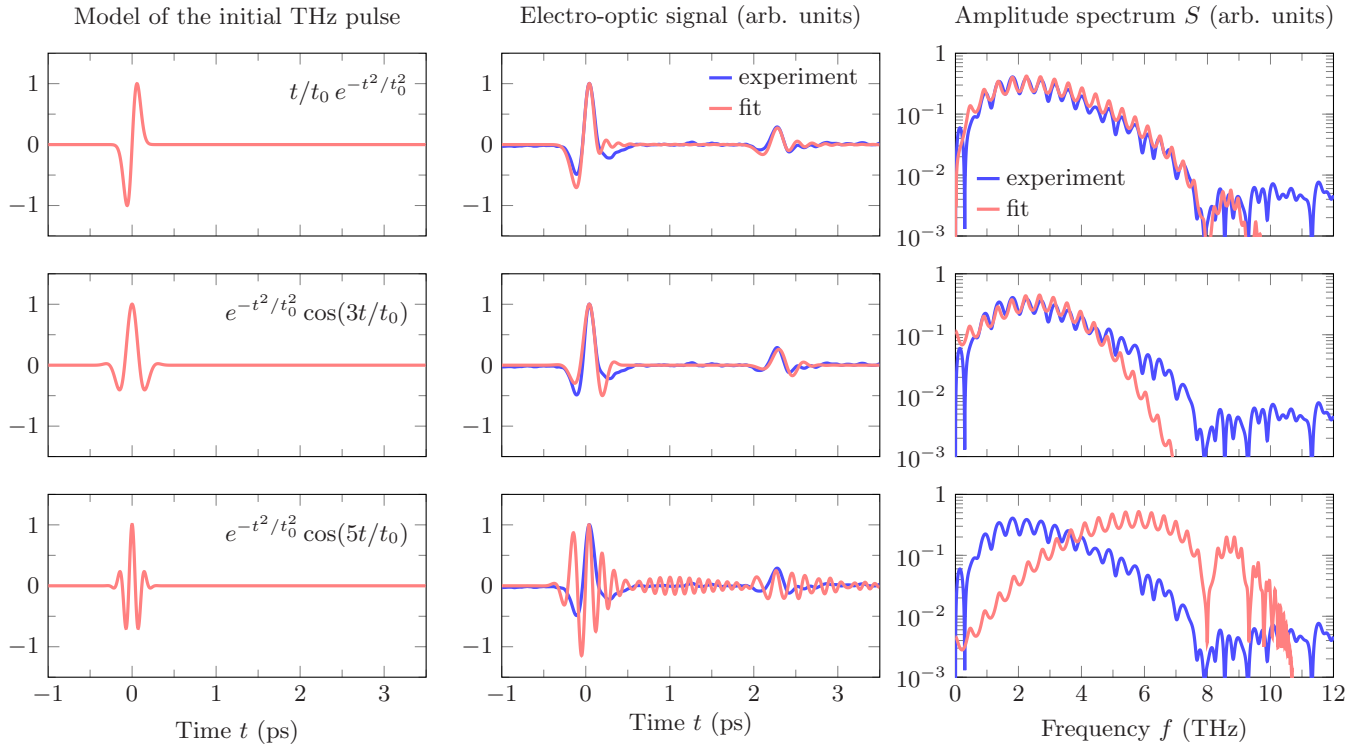


FIG. 3. The THz signal measured by  $100 \mu\text{m}$  GaP crystal (middle column) and its amplitude spectrum (right column) together with their best fits obtained by the reconstruction method for different models of the initial THz pulse (left column). The echoes seen in the measured fields (middle column) come from the finite thickness of the EO crystal and are actually useful in the fitting process since the resulting Fabry-Perot interference fringes in the spectra (right column) fix the thickness of the crystal.

$10^{13}$ – $10^{14}$  W/cm<sup>2</sup>, as well as for different  $I_{2\omega_0}/I_{\omega_0}$  ratios. We found that Eq. (11) is always valid with practically the same value of  $a$ , while  $b$  has a variance of  $\pm 5$  fs. This would suggest that if one uses Eq. (11) with our experimentally extracted values of  $a$  and  $b$  to calculate the THz pulse duration resulting from two-color filaments in gases under different experimental conditions, the obtained result would still be close to the real one within an error of 10–20%, which is something that we have validated with published results of ABCD measurements (that are closer to the real THz pulse durations) found in the literature [20,21,28].

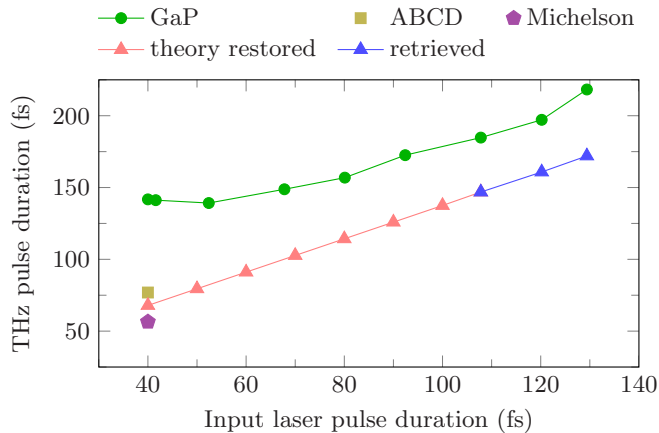


FIG. 4. THz pulse duration  $\tau_s$  measured with a GaP EO crystal (blue dots) and the corresponding restored duration  $\tau_0$  (red and green triangles), as a function of the input laser-pulse duration  $\tau_i$ .

## VI. ABSOLUTE AMPLITUDE OF THE THz PULSE

In the previous section, we have shown how to retrieve the shape and duration of the original THz pulse distorted by an EO detector. If, additionally, one can find a way to retrieve the absolute amplitude  $E_0$ , then all of the information about the original THz wave packet will be known. There are two standard methods to calculate the absolute amplitude  $E_0$  of a THz electric field if one uses EO detection. In order to apply the first method, we need to measure the total energy of a THz pulse. Additionally, for the same pulse, we need to measure its spatial distribution and EO signal, then normalize them and integrate. The desired amplitude  $E_0$  can be found if we divide the total THz energy by the two calculated integrals [29].

The second method is based on a simplified version of the theory of EO detection (see Sec. IV), where we neglect the dispersion inside the EO crystal. As a result of this simplification, we find that the peak of an EO signal corresponds to a relative phase shift  $\Gamma$  given by [23]

$$\Gamma = \frac{2\pi n_0^3 d}{\lambda_0} r_{41} E_0, \quad (12)$$

where  $r_{41}$  is calculated at some specific frequency. The resulting value of  $E_0$  is then calculated by Eq. (1), using the readings from the balanced photodiodes of the EO detection setup.

Both of these methods have substantial disadvantages. In the first method, we assume that the temporal distribution of the THz field is well represented by an EO signal, which, as we have already seen, is not true. Moreover, this method

demands additional measurements of the spatial profile of the THz pulse. In turn, the second method does not take into account the dispersion inside the EO crystal.

As an alternative to the existing methods, we can calculate the absolute amplitude of the THz electric field using our reconstruction method. The calculation stages are the following. First, using a normalized EO signal, we restore the duration  $\tau_0$  of the original THz pulse, thereby obtaining its shape, that is, its normalized electric field. Then, we simulate the EO signal for a THz pulse with the restored  $\tau_0$  and unity amplitude, say 1 kV/cm. As a result, for a given THz pulse with a given  $\tau_0$ , we find the relation between the absolute amplitude  $E_0$  (in physical units) and the peak value of the relative phase shift  $\Gamma$ . The final scaling can be done using Eq. (1) and the readings from the balanced photodiodes. Thus, our result will be the closest one to the actual value of the absolute amplitude, since it does not depend on additional measurements of the pulse profile and takes into account the distortions introduced by the EO detector including the dispersion of the EO crystal.

Following the above procedure, we find that our THz pulse with duration  $\tau_0 = 68$  fs has peak amplitude  $E_0$  equal to 250 kV/cm. For comparison, the amplitude calculated using Eq. (12) is equal to 70 kV/cm, which is three times lower than the value obtained by our reconstruction method.

## VII. CONCLUSIONS

In conclusion, we have shown that one can fully retrieve the ultrashort broadband THz wave packets produced by two-color laser filaments even when using dispersive and bandwidth lossy detection channels, such as the very popular electro-optic detection. This was made possible by identifying the THz spectrum bandwidth scaling laws as a function of the input laser-pulse duration and by correcting for the electro-optic detection distortions using an iterative nonlinear curve fitting algorithm. Our results beyond the evident impact on THz science and technology can open the way in suggesting similar solutions to other problems where only partial information of wave packets and wave functions can be measured.

## ACKNOWLEDGMENTS

We gratefully acknowledge the assistance of Mrs. Christiana Alexandridi on the Michelson interferometry data. This work was supported by the Greek General Secretariat for Research and Technology (GSRT) Aristeia project FTERA (Grant No. 2570), cofinanced by the European Union and Greek National Funds and the H2020 “Laserlab Europe” (Grant No. EC-GA 654148).

- 
- [1] M. Tonouchi, *Nat. Photon.* **1**, 97 (2007).
  - [2] B. Ferguson and X.-C. Zhang, *Nat. Mater.* **1**, 26 (2002).
  - [3] M. Jewariya, E. Abraham, T. Kitaguchi, Y. Ohgi, M.-a. Minami, T. Araki, and T. Yasui, *Opt. Express* **21**, 2423 (2013).
  - [4] M. Massaouti, C. Daskalaki, A. Gorodetsky, A. D. Koulouklidis, and S. Tzortzakakis, *Appl. Spectrosc.* **67**, 1264 (2013).
  - [5] J. Zhao, W. Chu, L. Guo, Z. Wang, J. Yang, W. Liu, Y. Cheng, and Z. Xu, *Sci. Rep.* **4**, 3880 (2014).
  - [6] J. M. Manceau, A. Nevin, C. Fotakis, and S. Tzortzakakis, *Appl. Phys. B* **90**, 365 (2008).
  - [7] D. Turchinovich, J. M. Hvam, and M. C. Hoffmann, *Phys. Rev. B* **85**, 201304 (2012).
  - [8] M. Zalkovskij, A. C. Strikwerda, K. Iwaszczuk, A. Popescu, D. Savastru, R. Malureanu, A. V. Lavrinenko, and P. U. Jepsen, *Appl. Phys. Lett.* **103**, 221102 (2013).
  - [9] J. Hebling, M. C. Hoffmann, K.-L. Yeh, G. Tóth, and K. A. Nelson, in *Ultrafast Phenomena XVI*, Springer Series in Chemical Physics, edited by P. Corkum, S. Silvestri, K. A. Nelson, E. Riedle, and R. W. Schoenlein (Springer, Berlin, Heidelberg, 2009), pp. 651–653.
  - [10] W. R. Huang, S.-W. Huang, E. Granados, K. Ravi, K.-H. Hong, L. E. Zapata, and F. X. Kärtner, *J. Mod. Opt.* **62**, 1 (2014).
  - [11] K. Y. Kim, A. J. Taylor, J. H. Glowina, and G. Rodriguez, *Nat. Photon.* **2**, 605 (2008).
  - [12] T. I. Oh, Y. S. You, N. Jhajj, E. W. Rosenthal, H. M. Milchberg, and K. Y. Kim, *Appl. Phys. Lett.* **102**, 201113 (2013).
  - [13] C. Vicario, A. V. Ovchinnikov, S. I. Ashitkov, M. B. Agranat, V. E. Fortov, and C. P. Hauri, *Opt. Lett.* **39**, 6632 (2014).
  - [14] T. I. Oh, Y. S. You, N. Jhajj, E. W. Rosenthal, H. M. Milchberg, and K. Y. Kim, *New J. Phys.* **15**, 075002 (2013).
  - [15] I. Brener, D. Dykaar, A. Frommer, L. N. Pfeiffer, J. Lopata, J. Wynn, K. West, and M. C. Nuss, *Opt. Lett.* **21**, 1924 (1996).
  - [16] Y. Cai, I. Brener, J. Lopata, J. Wynn, L. Pfeiffer, and J. Federici, *Appl. Phys. Lett.* **71**, 2076 (1997).
  - [17] Q. Wu and X.-C. Zhang, *Appl. Phys. Lett.* **67**, 3523 (1995).
  - [18] A. Nahata, D. H. Auston, T. F. Heinz, and C. Wu, *Appl. Phys. Lett.* **68**, 150 (1996).
  - [19] C. Kubler, R. Huber, and A. Leitenstorfer, *Semicond. Sci. Technol.* **20**, S128 (2005).
  - [20] J. Dai, J. Liu, and X.-C. Zhang, *IEEE J. Sel. Top. Quantum Electron.* **17**, 183 (2011).
  - [21] X. Lu and X.-C. Zhang, *Appl. Phys. Lett.* **98**, 151111 (2011).
  - [22] Z. Lü, D. Zhang, C. Meng, L. Sun, Z. Zhou, Z. Zhao, and J. Yuan, *Appl. Phys. Lett.* **101**, 081119 (2012).
  - [23] S. Casalbuoni, H. Schlarb, B. Schmidt, P. Schmäser, B. Steffen, and A. Winter, *Phys. Rev. Spec. Top. Accel. Beams* **11**, 072802 (2008).
  - [24] K.-Y. Kim, J. H. Glowina, A. J. Taylor, and G. Rodriguez, *Opt. Express* **15**, 4577 (2007).
  - [25] G. L. Yudin and M. Y. Ivanov, *Phys. Rev. A* **64**, 013409 (2001).
  - [26] A. V. Borodin, N. A. Panov, O. G. Kosareva, V. A. Andreeva, M. N. Esaulkov, V. A. Makarov, A. P. Shkurinov, S. L. Chin, and X. C. Zhang, *Opt. Lett.* **38**, 1906 (2013).
  - [27] M. Brunken, H. Genz, C. Hessler, H. Loos, A. Richter, P. Göttlicher, M. Hüning, H. Schlarb, S. Simrock, P. Schmäser, D. Suetterlin, M. Tonutti, and D. Türke, Electro-Optic Sampling at the TESLA Test Accelerator: Experimental Setup and First Results, TESLA Report No. 2003-11, 2003, [http://tesla.desy.de/new\\_pages/TESLA/TTFnot03.html](http://tesla.desy.de/new_pages/TESLA/TTFnot03.html).
  - [28] I. C. Ho and X. C. Zhang, *Front. Optoelectron.* **7**, 220 (2014).
  - [29] F. Blanchard, G. Sharma, X. Ropagnol, L. Razzari, R. Morandotti, and T. Ozaki, *Opt. Express* **17**, 6044 (2009).